Tm:CALGO lasers at 2.32 μm: cascade lasing and upconversion pumping

Hippolyte Dupont, Pavel Loiko, Aleksey Tyazhev, Luidgi Giordano, Zhongben Pan, Hongwei Chu, Dechun Li, Bruno Viana, Ammar Hideur, Lauren Guillemot, et al.

Research Article | Vol. 31, No. 12 / 5 Jun 2023 / Optics Express 18751
Optics EXPRESS

Tm:CALGO lasers at 2.32 µm: cascade lasing and upconversion pumping

HIPPOLYTE DUPONT,[1] PAVEL LOIKO,[2] ALEKSEY TYAZHEV,[3] LUIDGI GIORDANO,[4] ZHONGBEN PAN,[5] HONGWEI CHU,[5] DECHUN LI,[5] BRUNO VIANA,[4] AMMAR HIDEUR,[3] LAUREN GUILLEMOT,[2] ALAIN BRAUD,[2] PATRICE CAMY,[2] PATRICK GEORGES,[1] AND FRÉDÉRIC DRUON[1,*]

[1] *Université Paris-Saclay, Institut d'Optique Graduate School, CNRS, Laboratoire Charles Fabry, 91127 Palaiseau, France*
[2] *Centre de Recherche sur les Ions, les Matériaux et la Photonique (CIMAP), UMR 6252 CEA-CNRS-ENSICAEN, Université de Caen, 6 Boulevard Maréchal Juin, 14050 Caen Cedex 4, France*
[3] *CORIA UMR6614, CNRS-INSA-Université de Rouen, Normandie Université, Avenue de l'université, BP. 12, 76801 Saint Etienne du Rouvray, France*
[4] *Chimie ParisTech, PSL University, CNRS, Institut de Recherche de Chimie Paris, 11 rue Pierre et Marie Curie, 75005 Paris, France*
[5] *School of Information Science and Engineering, Shandong University, Qingdao 266237, China*
[*] *frederic.druon@institutoptique.fr*

Abstract: We report on the first laser operation of a disordered Tm:$CaGdAlO_4$ crystal on the $^3H_4 \rightarrow {}^3H_5$ transition. Under direct pumping at 0.79 µm, it generates 264 mW at 2.32 µm with a slope efficiency of 13.9% and 22.5% vs. incident and absorbed pump power, respectively, and a linear polarization (σ). Two strategies to overcome the bottleneck effect of the metastable $^3F_4$ Tm^{3+} state leading to the ground-state bleaching are exploited: cascade lasing on the $^3H_4 \rightarrow {}^3H_5$ and $^3F_4 \rightarrow {}^3H_6$ transitions and dual-wavelength pumping at 0.79 and 1.05 µm combining the direct and upconversion pumping schemes. The cascade Tm-laser generates a maximum output power of 585 mW at 1.77 µm ($^3F_4 \rightarrow {}^3H_6$) and 2.32 µm ($^3H_4 \rightarrow {}^3H_5$) with a higher slope efficiency of 28.3% and a lower laser threshold of 1.43 W, out of which 332 mW are achieved at 2.32 µm. Under dual-wavelength pumping, further power scaling to 357 mW at at 2.32 µm is observed at the expense of increased laser threshold. To support the upconversion pumping experiment, excited-state absorption spectra of Tm^{3+} ions for the $^3F_4 \rightarrow {}^3F_{2,3}$ and $^3F_4 \rightarrow {}^3H_4$ transitions are measured for polarized light. Tm^{3+} ions in $CaGdAlO_4$ exhibit broadband emission at 2.3 - 2.5 µm making this crystal promising for ultrashort pulse generation.

1. Introduction

Thulium ions (Tm^{3+}) possess an electronic configuration of $[Xe]4f^{12}$ with a ground-state $^3H_6$. There are two laser transitions of Tm^{3+} ions falling into the short-wave infrared spectral range, $^3F_4 \rightarrow {}^3H_6$ (at ~1.9 µm) and $^3H_4 \rightarrow {}^3H_5$ (at ~2.3 µm), Fig. 1. Laser sources emitting at 2.3 µm find applications in atmosphere gas sensing, pollutant detection, combustion studies and non-invasive glucose blood measurements [1,2]. They are also noteworthy for pumping of mid-infrared optical parametric oscillators [3]. Tm-lasers operating on the $^3H_4 \rightarrow {}^3H_5$ transition offer a good opportunity to cover this wavelength range [4].

So far, two main pumping schemes for Tm lasers operating on the $^3H_4 \rightarrow {}^3H_5$ transition were implemented: direct and upconversion pumping. *Direct* pumping at 0.8 µm relying on the $^3H_6 \rightarrow {}^3H_4$ ground-state absorption (GSA). This scheme leads to a direct excitation of Tm^{3+} ions to the upper laser manifold ($^3H_4$); the laser emission at 2.3 µm is followed by a fast NR relaxation from the short-living $^3H_5$ state and electronic excitations are accumulated in the metastable $^3F_4$

#487590 https://doi.org/10.1364/OE.487590
Journal © 2023 Received 16 Feb 2023; revised 27 Mar 2023; accepted 7 Apr 2023; published 22 May 2023

Optics EXPRESS

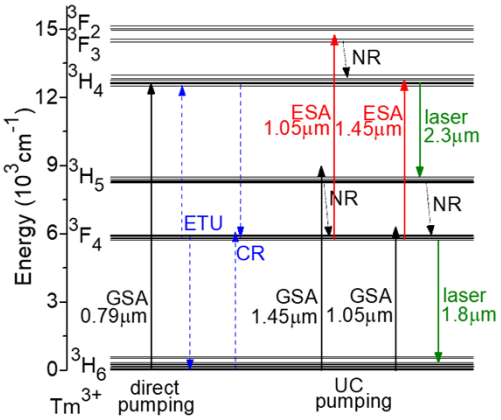

Fig. 1. A partial energy-level scheme for Tm^{3+} ions in $CaGdAlO_4$ ([32–42]) showing the direct and UC pumping schemes for achieving $^3H_4 \rightarrow {}^3H_5$ laser emission: GSA / ESA – ground / excited state absorption, CR – cross-relaxation, ETU – energy-transfer upconverison, NR – multiphonon non-radiative relaxation.

level. The ETU process, $^3F_4 + {}^3F_4 \rightarrow {}^3H_6 + {}^3H_4$, can assist in emptying the metastable manifold and refilling the upper laser level increasing the pump quantum efficiency up to 2 (a one-to-two process) [5]. Direct pumping is realized using AlGaAs laser diodes [6,7] or Ti:Sapphire lasers [8–10]. Guillemot *et al.* reported on a Tm:KY_3F_{10} laser with direct pumping delivering 0.84 W at 2.34 μm with a slope efficiency of 47.7% exceeding the Stokes limit [8].

Upconversion (UC) pumping [11,12] relies on a weak phonon-assisted $^3H_6 \rightarrow {}^3H_5 + h\nu_{ph}$ or $^3H_6 \rightarrow {}^3F_4 + h\nu_{ph}$ ground-state absorption, and a resonant $^3F_4 \rightarrow {}^3F_{2,3}$ (at 1 μm) or $^3F_4 \rightarrow {}^3H_4$ (at 1.45 μm) excited-state absorption, respectively. The ESA efficiency is boosted by the photon avalanche effect [13] which is driven by a combination of a resonant ESA and a cross-relaxation (CR) process, $^3H_4 + {}^3H_6 \rightarrow {}^3F_4 + {}^3F_4$, and it recycles the population of the $^3F_4$ level in favor of the upper laser level ($^3H_4$). UC pumping can be realized using commercial Yb bulk and fiber lasers featuring high brightness and high-power output. Upconversion pumping of bulk Tm^{3+}-doped crystals using Yb-fiber lasers was studied [11,14–16]. There are also reports on Tm-fiber lasers employing such a pumping scheme [12,17–19]. In particular, Tyazhev *et al.* reported on a Tm:ZBLAN fiber laser with UC pumping by an Yb-fiber laser generating 1.24 W at 2.28 μm with a slope efficiency of 37% [19].

The two pump schemes can also be combined for *dual-wavelength* pumping [20,21]. It was shown that even a small addition of direct pump can populate the metastable $^3F_4$ Tm^{3+} state resulting in a seeding effect for the $^3F_4 \rightarrow {}^3F_{2,3}$ excited-state absorption and leading to enhanced pump absorption at ~1 μm [20].

Another strategy to purge the metastable level consists in using cascade laser operation.

2. Cascade laser strategy

Cascade (or *cooperative*) *lasing* is a phenomenon when laser operation on one transition of an active center can facilitate lasing on another (desirable) laser transition [22–24]. It can be observed for centers with a metastable lower-lying excited-state $|1>$. Transitions from higher-lying excited-states terminating at this long-living intermediate level $|2> \rightarrow |1>$ can be of self-terminating nature [25]: if the lifetime of the terminal laser level is longer than that of the emitting state ($\tau_1 > \tau_2$), electronic excitations will be accumulated in the former manifold, and laser action will only be possible within a short period of time until the $|1>$ level is strongly populated so that the population inversion is no longer possible (*the bottleneck effect*). The laser

Optics EXPRESS

will then only operate in a pulsed regime (transient lasing). By allowing the gain medium to simultaneously operate on the $|1> \rightarrow |0>$ transition ($|0>$ is the ground-state), the intermediate manifold $|1>$ will be efficiently depopulated, Fig. 2(a).

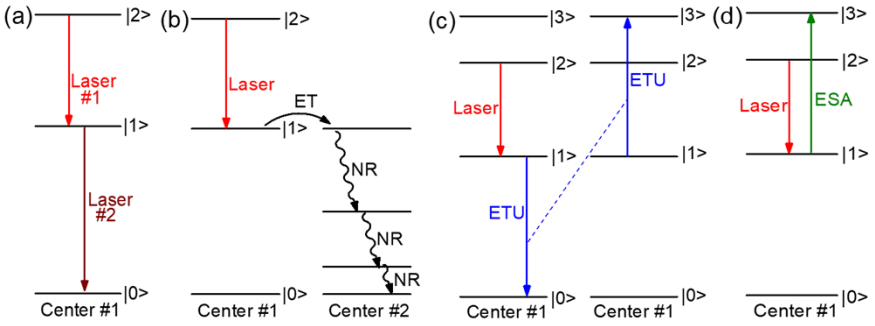

Fig. 2. Different approaches to avoid the bottleneck effect for laser-active centers: (a) cascade lasing, (b) codoping with a quenching center, (c) energy-transfer upconversion (ETU) and (d) excited-state absorption (ESA).

Other possibilities to overcome the bottleneck effect include codoping of the gain medium with a different type of optical centers causing quenching of the $|1>$ level lifetime due to a non-radiative energy-transfer followed by a multi-phonon non-radiative (NR) relaxation [26], the use of high doping levels triggering efficient energy-transfer upconversion (ETU) from the metastable level $|1>$ emptying it [27], or the use of excited-state absorption (ESA) from the $|1>$ level for the same purpose, see Fig. 2(b-d).

Cascade lasing was described for several rare-earth ions (RE^{3+}) with a metastable lower-lying excited-state, acting as a reservoir for electronic excitations, namely Er^{3+} [22], Tm^{3+} [24], Ho^{3+} [23,28] and Dy^{3+} [29], Fig. 3. Besides the main purpose of allowing the population inversion for the desirable $|2> \rightarrow |1>$ transition, cascade lasing also helps to avoid excessive bleaching of the ground-state (by preventing accumulation of electronic excitations in the $|1>$ manifold) which could potentially reduce the pump absorption efficiency.

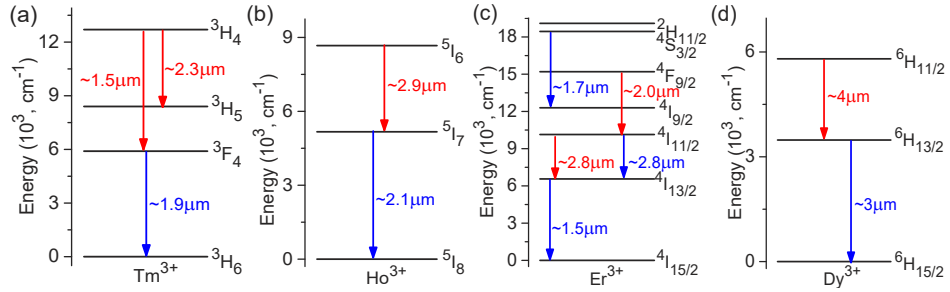

Fig. 3. Cascade lasing schemes for trivalent rare-earth ions: (a) thulium, (b) holmium, (c) erbium and (d) dysprosium. *Red arrows* –laser transitions subject to the bottleneck effect, *blue arrows* – assisting transitions from a metastable state.

3. $CaGdAlO_4$ laser host crystals

One of the key limitations for the development of broadly tunable or femtosecond mode-locked Tm lasers operating on the $^3H_4 \rightarrow {}^3H_5$ transition [30,31] is the need of gain media featuring

Optics EXPRESS

broadband emission properties. Such behavior can be achieved for structurally disordered crystal with a strong inhomogeneous broadening of Tm^{3+} spectral bands.

Calcium gadolinium aluminate $CaGdAlO_4$ (shortly CALGO) is a well-known laser host crystal [32–37]. It crystallizes in the tetragonal class (sp. gr. D^{17}_{4h} - *I4/mmm*, lattice constants: $a = 3.66052(9)$ Å, $c = 11.986(5)$ Å [38]) possessing a K_2NiF_4-type structure and exhibits a structure disorder due to a random distribution of Ca^{2+} and Gd^{3+} cations over the same lattice sites (Wyckoff: 4*e*, C_{4v} symmetry) with an IX-fold oxygen coordination. The dopant RE^{3+} ions replace for the Gd^{3+} ones. The inhomogeneous spectral broadening originates from the second coordination sphere of the RE^{3+} ions composed of nine cations ($Ca^{2+}|Gd^{3+}$) in 4*e* sites, namely the charge difference between Ca^{2+} and Gd^{3+}, as well as a notable difference in the metal-to-metal distances [32].

$CaGdAlO_4$ melts congruently and can be growth by the conventional Czochralski method. As a host matrix, $CaGdAlO_4$ features good thermal properties, *i.e.*, high thermal conductivity despite its disordered nature with a moderate dependence on the RE^{3+} doping level, negative dn/dT coefficients leading to an *athermal* behavior, and a weak anisotropy of thermal expansion [33]. Such properties favor high-power laser operation [34]. The relatively low phonon energy of $CaGdAlO_4$ (among oxide crystals) leads to reduced NR path from the RE^{3+} excited states. A summary of physical properties of the $CaGdAlO_4$ host crystal is given in Table 1. RE^{3+} ions in $CaGdAlO_4$ feature extremely broad and smooth emission spectra for polarized light which is attractive for the development of broadly tunable and especially few-optical-cycle mode-locked lasers [35–37].

Table 1. Structural, Thermal, Vibronic and Optical Properties of the $CaGdAlO_4$ Host Crystal

Parameter	Notation	Units	Value	Ref.
Lattice constants	A	[Å]	3.66052(9)	[38]
	c		11.986(5)	
Refractive index (at ~1 µm)	n_o	-	1.918	[42]
	n_e		1.941	
Thermo-optic coefficient (at ~1 µm)	dn_o/dT	[10^{-6} K^{-1}]	-7.6	[33]
	dn_e/dT		-8.6	
Thermal expansion	α_a	[10^{-6} K^{-1}]	10.0	[33]
	α_c		16.0	
Thermal conductivity (2 at.% Yb)	κ_a	[Wm^{-1}K^{-1}]	6.9	[33]
	κ_c		6.3	
Maximum phonon energy	$h\nu_{ph}$	[cm^{-1}]	650	[39]

So far, Yb^{3+}-doped $CaGdAlO_4$ crystals have been recognized as excellent gain media for high-power ultrafast lasers at ~1 µm [35–37]. More recently, the interest shifted to Tm^{3+} doping with the goal of achieving laser emission around 2 µm [39–41].

In the present work, we aimed to further explore the broadband emission properties of Tm^{3+} ions in the $CaGdAlO_4$ crystal by looking at the $^3H_4 \rightarrow {}^3H_5$ transition. First, we studied the emission and absorption (including excited-state absorption) properties of Tm^{3+} ions in this material. Then, laser operation at 2.3 µm was achieved for the first time using direct and dual-wavelength pumping. Finally, we studied the effect of cascade lasing on the $^3H_4 \rightarrow {}^3H_5$ and $^3F_4 \rightarrow {}^3H_6$ transitions on the 2.3 µm laser performance.

Optics EXPRESS

4. Spectroscopy of Tm^{3+} ions

4.1. Ground- and excited-state absorption

Tetragonal $CaGdAlO_4$ is optically uniaxial (the optical axis is parallel to the ***c***-axis) [42] and the two principal light polarizations are π (***E*** || ***c***) and σ (***E*** ⊥ ***c***).

The polarized ground-state absorption (GSA) cross-sections, σ_{GSA}, for the $^3H_6 \rightarrow {}^3H_4$ Tm^{3+} transition (direct pumping) are shown in Fig. 4(a) [39]. The maximum σ_{GSA} is 1.59×10^{-20} cm^2 at 792.4 nm and the absorption bandwidth (full width at half maximum, FWHM) is 16.3 nm for π-polarization. For σ-polarization, σ_{GSA} is lower, 0.68×10^{-20} cm^2 at 797.8 nm.

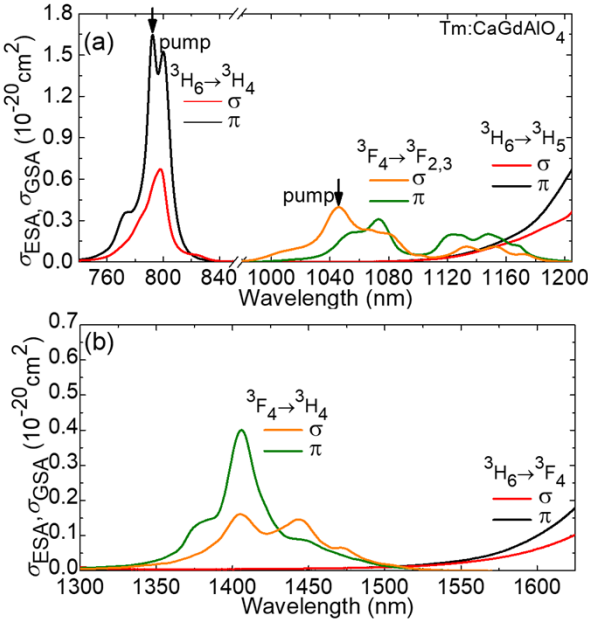

Fig. 4. Polarized absorption properties of Tm^{3+} ions in $CaGdAlO_4$: (a) GSA cross-sections, σ_{GSA}, for the $^3H_6 \rightarrow {}^3H_4$ transition and ESA cross-sections, σ_{ESA}, for the $^3F_4 \rightarrow {}^3F_{2,3}$ transition; (b) ESA cross-sections, σ_{ESA}, for the $^3F_4 \rightarrow {}^3H_4$ transition, for light polarizations π and σ. The short-wave sidebands of spectrally overlapping GSA transitions essential for seeding the photon avalanche effect are also shown for comparison. *Arrows* indicate the pump wavelengths.

The polarized ESA spectra of Tm^{3+} ions in the near-infrared are measured in the present work by the pump-probe method and polarized light [43]. Two ESA transitions originating from the metastable Tm^{3+} manifold ($^3F_4$) relevant for upconversion pumping of 2.3 μm Tm-lasers are considered, namely $^3F_4 \rightarrow {}^3F_{2,3}$ and $^3F_4 \rightarrow {}^3H_4$. The ESA cross-sections, σ_{ESA}, are given in Fig. 4(a,b). The spectra are smooth and broad owing to a significant inhomogeneous spectral line broadening caused by the local structure disorder in the $CaGdAlO_4$ crystal.

For the $^3F_4 \rightarrow {}^3F_{2,3}$ transition which can be addressed by Yb lasers, the maximum σ_{ESA} reaches 0.40×10^{-20} cm^2 at 1045.9 nm corresponding to a large peak width (FWHM) of 25.2 nm for σ-polarization, see Fig. 4(a). For π-polarization, ESA is weaker, as expressed by $\sigma_{ESA} = 0.31 \times 10^{-20}$ cm^2 at 1073.1 nm also corresponding to a narrower peak width of 19.2 nm. This ESA band spectrally overlaps with the short-wave phonon sideband of the $^3H_6 \rightarrow {}^3H_5$ GSA transition. At the peak ESA wavelength of 1045.9 nm, the corresponding σ_{GSA} is as low as 0.07×10^{-22} cm^2 for σ-polarization. Despite the very weak GSA, it is sufficient to initiate the photon avalanche mechanism underlying the upconversion pumping scheme of 2.3 μm Tm-lasers.

Optics EXPRESS

For the second considered $^3F_4 \rightarrow {}^3H_4$ ESA transition, σ_{ESA} is 0.40×10^{-20} cm^2 at 1405.9 nm with a peak FWHM of 26.5 nm for π-polarization, see Fig. 4(b). For σ-polarization, two weaker ESA peaks are found at 1405.2 and 1443.6 nm corresponding to σ_{ESA} of 0.15-0.16 $\times 10^{-20}$ cm^2. This ESA band overlaps with the short-wave phonon sideband of the $^3H_6 \rightarrow {}^3F_4$ GSA transition.

4.2. Emission (spectra and lifetimes)

The stimulated-emission (SE) cross-sections, σ_{SE}, for the $^3F_4 \rightarrow {}^3H_6$ and $^3H_4 \rightarrow {}^3H_5$ transitions are shown in Fig. 5(a). The σ_{SE} spectra are smooth and broad extending in the spectral ranges of 1.6–2.1 μm and 2.15–2.65 μm, respectively, and they show a polarization anisotropy which is a prerequisite for linearly polarized laser emission.

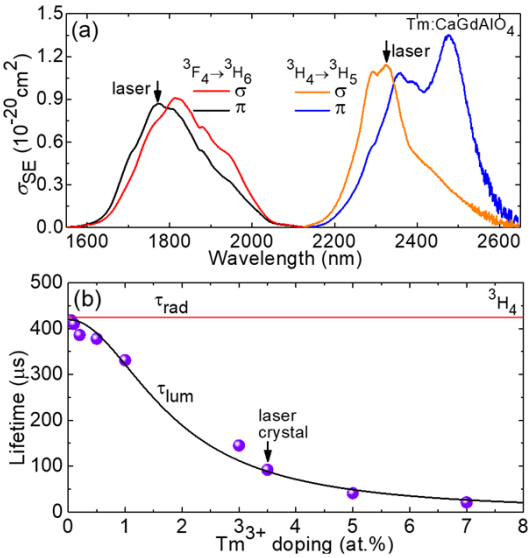

Fig. 5. Emission properties of Tm^{3+} ions in $CaGdAlO_4$: (a) SE cross-sections, σ_{SE}, for the $^3F_4 \rightarrow {}^3H_6$ and $^3H_4 \rightarrow {}^3H_5$ transitions for light polarizations π and σ; (b) the luminescence lifetime of the $^3H_4$ level as a function of the Tm^{3+} doping level (*symbols* – experimental data, *curve* – their fit accounting for the cross-relaxation among adjacent Tm^{3+} ions, see the explanations in the text). *Arrows* in (a) indicate the laser wavelengths.

For the $^3F_4 \rightarrow {}^3H_6$ transition, the peak stimulated emission cross-sections are 0.91×10^{-20} cm^2 at 1812nm for σ-polarization, and 0.87×10^{-20} cm^2 at 1774nm for π-polarization [34]. Due to the quasi-three-level nature of the $^3F_4 \rightarrow {}^3H_6$ Tm^{3+} transition with intrinsic reabsorption, when using cavity mirrors with broadband coatings, the laser operation usually occurs at the long-wave part of the σ_{SE} spectrum, and the laser wavelength is determined by a local maximum in the gain profile for a particular inversion ratio determined by the total (passive and output-coupling) losses. For Tm^{3+} ions in $CaGdAlO_4$, for small inversion ratios, this corresponds to a local peak at 1948nm ($\sigma_{SE} = 0.50 \times 10^{-20}$ cm^2, σ-polarization).

For the quasi-four-level $^3H_4 \rightarrow {}^3H_5$ transition, the SE cross-sections are derived in the present work via the Füchtbauer–Ladenburg (F-L) equation [44]:

$$\sigma_{SE}^{i}(\lambda) = \frac{\lambda^5}{8\pi\langle n\rangle^2 \tau_{rad} c} \cdot \frac{\beta_{JJ'} \cdot W_i(\lambda)}{\frac{1}{3}\sum_{j=2\sigma,\pi} \int \lambda W_j(\lambda) d\lambda}, \quad (1)$$

where $W_i(\lambda)$ the luminescence spectrum for each light polarization ($i = \sigma, \pi$), $<n>$ the average refractive index at the mean emission wavelength, τ_{rad} the radiative lifetime of the emitting

Optics EXPRESS

state ($^3H_4$), and $\beta_{JJ'}$ the luminescence branching ratio. Pan et al. reported on the Judd-Ofelt analysis for Tm^{3+} ions in $CaGdAlO_4$ yielding $\tau_{rad}(^3H_4) = 0.42$ ms and $\beta(^3H_4 \rightarrow {}^3H_5) = 3.0\%$ [39]. For σ-polarized light, the maximum SE cross-section is 1.14×10^{-20} cm^2 at 2324 nm and the emission bandwidth (FWHM) reaches 128 nm. For π-polarization, around 2.3 µm, the peak σ_{SE} is 1.08×10^{-20} cm^2 at 2358 nm while at longer wavelengths, an intense peak appears at 2478 nm corresponding to σ_{SE} is 1.35×10^{-20} cm^2 and an emission bandwidth as broad as 100 nm.

We also studied the luminescence lifetimes τ_{lum} of the $^3H_4$ and $^3F_4$ states of Tm^{3+} ions in $CaGdAlO_4$ as a function of the doping level (0.05–7 at.% Tm). The samples are finely powdered to avoid the effect of reabsorption (radiation trapping). The intrinsic lifetime of the $^3F_4$ Tm^{3+} level is 3.08 ms (for 0.05 at.% Tm). For the studied laser crystal with 3.5 at.% Tm, almost negligible luminescence quenching was observed. The concentration-dependence of τ_{lum} for the $^3H_4$ Tm^{3+} level (the upper laser level for the 2.3 µm laser transition) is shown in Fig. 5(b). With increasing the Tm^{3+} doping level, τ_{lum} gradually decreases from 418 to 21 µs indicating an enhanced effect of cross-relaxation (self-quenching) among adjacent Tm^{3+} ions, $^3H_4 + {}^3H_6 \rightarrow {}^3F_4 + {}^3F_4$, Fig. 1. The luminescence lifetime of the $^3H_4$ state can be expressed as $(1/\tau_{lum}) = (1/\tau_{lum,0}) + W_{CR}$, where $W_{CR} = C_{CR}N_{Tm}{}^2$ is the cross-relaxation rate and C_{CR} is the concentration-independent parameter [45]. The best fit of the experimental lifetimes with this equation, see the curve in Fig. 5(b), yields $\tau_{lum,0} = 420 \pm 5$ µs and $C_{CR} = 0.45 \pm 0.05 \times 10^{-37}$ $s^{-1}cm^6$.

5. Laser operation at 2.3 µm

5.1. Laser set-up

A 3.5 at.% Tm:$CaGdAlO_4$ (Tm:CALGO) crystal is used as a gain medium. The Tm^{3+} ion density N_{Tm} is then 4.31×10^{20} at/cm^3. A rectangular sample is cut from the annealed crystal. The crystal is oriented for light propagation along the ***a***-axis (***a***-cut) and has an aperture of 3.0×3.0 mm^2 for a thickness of 6.0 mm. Both its faces are polished to laser-grade quality with good parallelism and left uncoated. The crystal is mounted in a passively-cooled copper-mount using indium foil to insure good thermal contact.

The layout of the laser set-up is depicted in Fig. 6. A nearly hemispherical laser cavity uses a flat dichroic pump mirror transmitting the pump radiation (HT, $T > 95\%$ at 0.77-0.81 µm and 1.03-1.06 µm) and reflecting the laser emission (HR, $R > 99.9\%$ at 2.15-2.55 µm), and concave output couplers (OCs) with a radius of curvature (RoC) of -100 mm and a transmission T_{OC} in the range 0.5% - 4% at 2.20-2.45 µm. The crystal is placed close to the pump mirror at normal incidence with a small separation (~1 mm). The geometrical cavity length is ~99 mm.

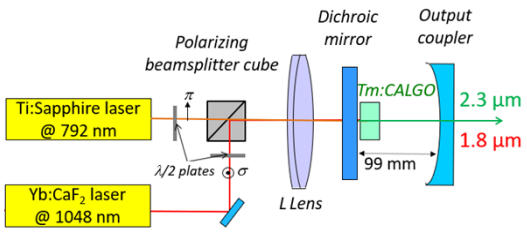

Fig. 6. Scheme of the dual-wavelength-pumped 2.3 µm Tm:$CaGdAlO_4$ laser.

In order to select laser action uniquely the $^3H_6 \rightarrow {}^3H_4$ transition or cascade laser operation, two sets of mirrors are used. First, to avoid the competitive high-gain $^3F_4 \rightarrow {}^3H_6$ transition, both the pump mirror and the output couplers are coated for HT ($T > 70\%$) at 1.9 µm. Second, to specifically study cascade laser operation, cavity mirrors allowing for dual-band operation are employed comprising a flat dichroic pump mirror coated for HR at 2.1-2.5 µm and 1.76-1.88 µm

Optics EXPRESS

and an output coupler with still RoC = -100 mm and a transmission T_{OC} of 2.5% at 2.32 µm and 10% at 1.77 µm.

For direct pumping, as a pump source, we use a CW Ti:Sapphire laser (model 3900S, Spectra Physics) delivering up to 3.9 W at 792.2 nm (with a FWHM linewidth of 0.1 nm) addressing the $^3H_6 \rightarrow {}^3H_4$ GSA transition with a linear polarization and a nearly diffraction limited beam ($M^2 \approx 1$). Its output is focused into the crystal through the pump mirror using an antireflection (AR) coated lens (focal length: f = 75 mm) resulting in a pump spot radius of 31 ± 5 µm. The polarization of the direct pump corresponded to π in the crystal.

For dual-wavelength pumping, we additionally employ a home-made diode-pumped tunable Yb:CaF_2 laser delivering up to 1.8 W at 1048 nm (with a FWHM linewidth of 3 nm) and with $M^2 \approx 1$ to address the $^3F_4 \rightarrow {}^3F_{2,3}$ ESA transition. The output of the Yb-laser is also linearly polarized. The polarization is adjusted to correspond to σ in the crystal. The two pump beams can be combined using a polarizing beam-splitter cube (PBS252, Thorlabs). The pump radiation is focused into the crystal through the pump mirror using an AR-coated lens (f = 80 mm) resulting in a waist radius of 35 ± 5 µm.

The residual pump after the OC is filtered out using a band-pass filter (FB2250-500 or FB1750-500, Spectrogon). The laser emission spectra are measured using an optical spectrum analyzer (AQ6375B, Yokogawa). The polarization state of laser emission is studied using a Glan-Taylor prism.

5.2. Direct pumping: pure 2.3 µm laser

At first, we study laser operation uniquely on the $^3H_6 \rightarrow {}^3H_4$ transition with pure direct pumping at 792 nm (addressing the $^3H_6 \rightarrow {}^3H_4$ GSA transition), Fig. 7(a). The output couplers coated for high transmission around 1.9 µm are used and no simultaneous laser action on the $^3F_4 \rightarrow {}^3H_6$ Tm^{3+} transition is observed.

The Tm:$CaGdAlO_4$ laser generates up to 264 mW of output power at 2301-2325 nm for the output coupler with a transmission of 2.5%. The corresponding slope efficiency η is 16.2% vs. the pump power incident on the crystal and the laser threshold is 1.77 W (for $T_{OC} = 2.5\%$), Fig. 7(a). This corresponded to a maximum incident pump power of 3.60 W and an optical efficiency of 7.3%. Further power scaling seems to be limited by the available pump power. No signs of thermal effects are observed within the studied range of pump powers. Accounting for the measured pump absorption under lasing conditions (see below), the slope efficiency vs. the absorbed pump power is 31.3% (i.e., close to the Stokes efficiency under lasing conditions, $\eta_{St,L} = \lambda_P/\lambda_L = 34.1\%$). This indicates that the effect of ETU on refilling the upper laser level is relatively weak in Tm:$CaGdAlO_4$.

The input-output dependences are slightly nonlinear above the laser threshold. The latter gradually increases with the output coupling, from 1.03 W ($T_{OC} = 0.5\%$) to 2.49 W ($T_{OC} = 4\%$). The laser threshold as a function of the output coupler transmission was simulated numerically using a rate-equation model accounting for the energy-transfer processes for Tm^{3+} ions, cf. Figure 1. The spectroscopic parameters of Tm^{3+} ions in $CaGdAlO_4$ described above were used in these calculations. The results are shown in Fig. 7(c) and they agree well with the experimental data. The relative high laser thresholds (e.g., as compared to Tm-lasers operating on the $^3H_4 \rightarrow {}^3H_5$ transition and based on fluoride crystals) mainly originate from the relatively short lifetime of the $^3H_4$ upper laser level, as well as weak ETU.

The typical spectra of laser emission measure well above the laser threshold are shown in Fig. 7(b). They are weakly dependent on the output coupling in accordance with the quasi-four-level $^3H_4 \rightarrow {}^3H_5$ Tm^{3+} laser scheme. The laser emission occurs around 2.32 µm according to the stimulated-emission cross-section spectra, Fig. 5(a). The laser spectra are relatively broad due to the broadband emission properties of Tm^{3+} ions in the disordered $CaGdAlO_4$ crystal; the multiple laser lines can be attributed to Fabry-Perrot effects at the mirror / crystal interfaces.

Optics EXPRESS

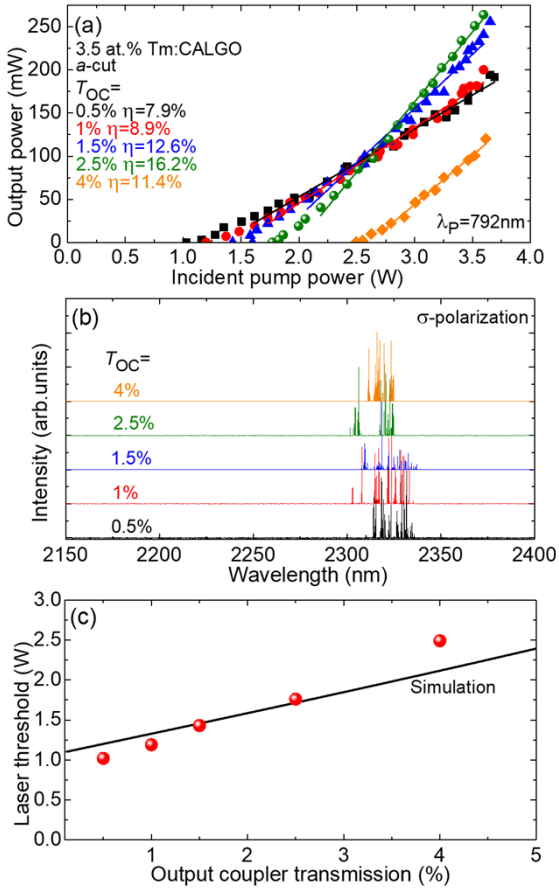

Fig. 7. Tm:CaGdAlO$_4$ laser operating on the $^3H_4 \rightarrow {}^3H_5$ transition at 2.32 μm, direct pumping at 792 nm (the $^3H_6 \rightarrow {}^3H_4$ GSA transition): (a) input-output dependences, η – slope efficiency; (b) typical spectra of laser emission, the laser polarization is σ; (c) laser threshold as a function of output coupling, *circles* - the experimental points, curve – result of the modeling based on rate-equation formalism.

This was confirmed by slightly changing the distance between the pump mirror and the crystal, as well as by changing the pump power which caused thermal expansion of the crystal (in both cases, the individual laser lines slightly shifted). This behavior is typical for free-running CW Tm:CaGdAlO$_4$ lasers [46]. Narrow-linewidth operation can be achieved by inserting a thin etalon into the laser cavity. The laser emission is linearly polarized (σ) since the polarization state is naturally selected by the gain anisotropy.

5.3. *Direct pumping: effect of cascade laser*

Cascade laser operation on the $^3H_4 \rightarrow {}^3H_5$ and $^3F_4 \rightarrow {}^3H_6$ Tm^{3+} transitions can be beneficial for power scaling of 2.3 μm Tm-lasers [47]. Indeed, it can help to drain the metastable intermediate $^3F_4$ Tm^{3+} state accumulating electronic excitations and causing bleaching of the ground-state ($^3H_6$) leading to a reduced pump absorption (GSA) efficiency. At the same time, simultaneous lasing on the $^3F_4 \rightarrow {}^3H_6$ transition may also cancel the positive effect of the energy-transfer upconversion process ($^3F_4 + {}^3F_4 \rightarrow {}^3H_6 + {}^3H_4$) refilling the upper laser level for the 2.3 μm laser transition ($^3H_4$).

Optics EXPRESS

To demonstrate cascade laser operation, cavity mirrors allowing for dual-band operation are employed. We use a flat pump mirror coated for HT at 0.79 µm and HR around 1.8 µm and 2.1-2.5 µm and a concave (RoC = -100 mm) output coupler with a transmission T_{OC} of 2.5% at 2.32 µm and 10% at 1.77 µm. To measure the total output power after the OC, a long-pass filter (LP1400, Thorlabs) is used, and to separate the power fraction of the $^3H_4 \rightarrow {}^3H_5$ laser emission, we employ a bandpass filter (FB2250-500, Spectrogon).

The cascade Tm:$CaGdAlO_4$ laser generated a maximum output power of 585 mW at 1760-1772nm ($^3F_4 \rightarrow {}^3H_6$) and 2297-2335 nm ($^3H_4 \rightarrow {}^3H_5$) with a slope efficiency of 28.3% and a laser threshold of 1.43 W, Fig. 8(a). For the $^3F_4 \rightarrow {}^3H_6$ transition at 1.77 µm, the maximum output power reaches 181 mW for a slope efficiency of 7.7%. The laser emission on the $^3H_4 \rightarrow {}^3H_5$ emission at 2.32 µm corresponds to 332 mW and a slope efficiency of 16.3%. Compared to the case of laser operation solely on the $^3H_4 \rightarrow {}^3H_5$ transition, cf. Figure 7(a), the laser threshold notably decreases leading to a higher output power.

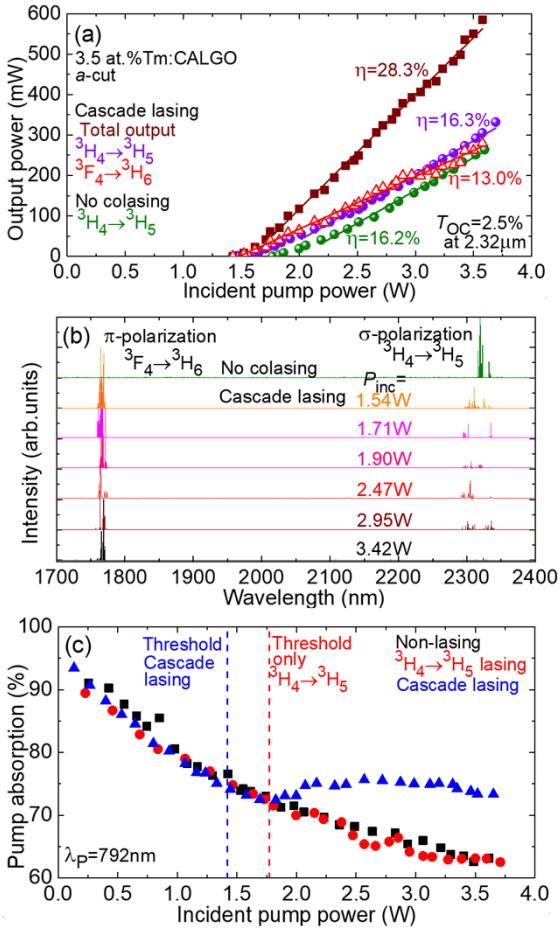

Fig. 8. Effect of cascade laser operation on the $^3H_4 \rightarrow {}^3H_5$ and $^3F_4 \rightarrow {}^3H_6$ transitions at 2.32 µm and 1.77 µm, respectively, on the output performance of a Tm:$CaGdAlO_4$ laser with a pure direct pumping at 792 nm: (a) input-output dependences for T_{OC} = 2.5% / 10% at 2.32 µm / 1.77 µm; (b) laser emission spectra at different incident pump powers P_{inc}: the laser polarization is σ ($^3H_4 \rightarrow {}^3H_5$) and π ($^3F_4 \rightarrow {}^3H_6$), *green curve* - experimental results from Section 3.2; (c) measured pump absorption as a function of the incident pump power for lasing and non-lasing conditions.

Optics EXPRESS

The typical spectra of emission from the cascade laser are shown in Fig. 8(b). They are weakly dependent on the incident pump power. The emission corresponding to the $^3F_4 \rightarrow {}^3H_6$ and $^3H_4 \rightarrow {}^3H_5$ transitions are under orthogonal laser polarizations, π and σ, in agreement with the anisotropy of SE cross-sections, Fig. 5(a).

The pump absorption as a function of the incident pump power is studied under lasing and non-lasing conditions, Fig. 8(c). In the latter case, it gradually dropped upon increasing the pump level representing the ground-state ($^3F_4$) bleaching. A similar tendency is observed for the Tm-laser operating solely on the $^3H_4 \rightarrow {}^3H_5$ transition because of accumulation of electronic excitations in the intermediate $^3F_4$ Tm^{3+} state. For the cascade laser, the pump absorption is nearly clamped well above the laser threshold due to the positive effect of the laser action on the $^3F_4 \rightarrow {}^3H_6$ transition emptying the $^3F_4$ manifold. This leads to a lower threshold pump power for the cascade laser, as well as a higher 2.3 μm output power, as shown in Fig. 8(a).

5.4. Upconversion pumping

Another approach to avoid the accumulation of electronic excitations in the intermediate long-living $^3F_4$ Tm^{3+} state affecting the pump absorption is to employ pure UC pumping at 1.05 μm or dual-wavelength pumping at 0.79 and 1.05 μm combining both the direct and UC pumping schemes. The $^3F_4 \rightarrow {}^3F_{2,3}$ ESA transition helps to recycle the population of the $^3F_4$ manifold in favor of the upper laser level for the $^3H_4 \rightarrow {}^3H_5$ transition.

First, we try to achieve laser operation at 2.3 μm under pure UC pumping but the laser threshold is not reached up to at least the incident pump power of 2 W.

Consequently, we proceed with the dual-wavelength pumping. The cavity mirrors supporting cascade laser emission are then implemented. The input-output dependences for the cascade Tm:$CaGdAlO_4$ laser with pumping simultaneously at 0.79 and 1.05 μm are shown in Fig. 9. First, the $P_{1.05}$ μm value is fixed and $P_{0.79}$ μm is varied, Fig. 9(a). By adding more UC pump, the output power at 2.32 μm (the $^3H_4 \rightarrow {}^3H_5$ transition) gradually increases while that at 1.77 μm (the $^3F_4 \rightarrow {}^3H_6$ transition) remains almost unchanged. For example, when $P_{0.79}$ μm was

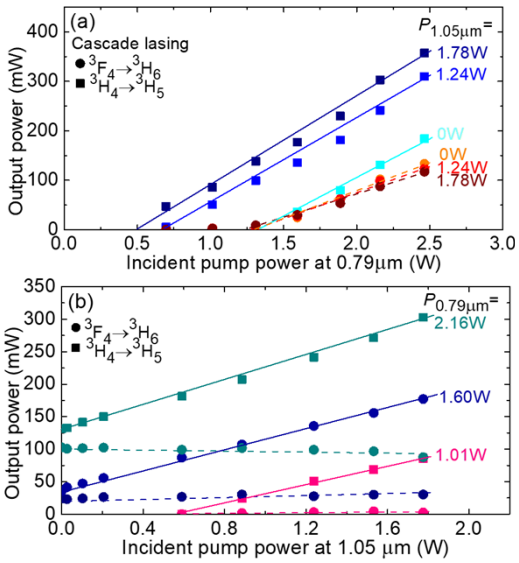

Fig. 9. Cascade (the $^3H_4 \rightarrow {}^3H_5$ and $^3F_4 \rightarrow {}^3H_6$ Tm^{3+} transitions) Tm:$CaGdAlO_4$ laser with dual-wavelength pumping at 0.79 and 1.05 μm: output powers at 1.77 μm and 2.32 μm: (a) $P_{0.79}$ μm – varied, $P_{1.05}$ μm – fixed; (b) $P_{0.79}$ μm – fixed, $P_{1.05}$ μm – varied.

Optics EXPRESS

fixed at 2.5 W (direct pump), by adding 1.78 W of $P_{1.05}$ µm (UC pump), the output power of the Tm-laser at 2.32 µm increases from 183 mW to 360 mW. At the same time, the laser threshold in terms of $P_{0.79}$ µm decreases from 1.45 W to 0.50 W (while considering the total incident pump power, $P_{0.79}$ µm + $P_{1.05}$ µm, the laser threshold increases). In other words, the reduction of the laser threshold in terms of $P_{0.79}$ µm (the positive effect) is lower than the additional pump power added at 1.05 µm, so that the UC pump des not help the direct pump to be more efficient.

Then, the opposite case is investigated: the $P_{0.79}$ µm value is fixed and $P_{1.05}$ µm is varied, Fig. 9(b). A similar effect is observed: the co-pumping at 0.79 µm has a positive effect on the output power at 2.32 µm and almost did not affect that at 1.77 µm. In this way, it is possible to tune the power fraction between the two laser emissions. The following explanation is suggested: the $^3F_4 \rightarrow {}^3F_{2,3}$ ESA transition drains a part of the population of the metastable $^3F_4$ Tm^{3+} level in favor of the $^3H_4 \rightarrow {}^3H_5$ emission. Under these conditions, the maximum output powers are 357 mW at 2.32 µm and 117 mW at 1.77 µm (total output: 474 mW) at an incident pump power of 4.24 W (total, at 0.79 and 1.05 µm).

6. Conclusions

To conclude, we report on the first laser operation of the thulium-doped calcium gadolinium aluminate crystal (Tm:$CaGdAlO_4$) on the $^3H_4 \rightarrow {}^3H_5$ Tm^{3+} electronic transition, at 2.3 µm. The main results can be summarized as follows:

Tm^{3+} ions in $CaGdAlO_4$ feature structureless and broad emission bands due to a significant inhomogeneous broadening arising from the structure disorder, together with a polarization anisotropy which is a prerequisite for linearly polarized laser emission. For σ-polarized light, the maximum stimulated emission cross-section is 1.14×10^{-20} cm^2 at 2324 nm and the emission bandwidth is as broad as 128 nm. This makes Tm:$CaGdAlO_4$ very suitable for broadly tunable and femtosecond mode-locked lasers. Moreover, this compound appears attractive for laser emission at yet longer wavelengths, at ~2.48 µm. Due to its low-phonon energy behavior, Tm^{3+} ions in CALGO exhibit a relatively long intrinsic lifetime of the $^3H_4$ state, 418 µs, being advantageous for low-threshold laser operation.

Another spectroscopic advantage arises from the broad and relatively intense ESA spectra of Tm^{3+} ions slightly above 1 µm (corresponding to the $^3F_4 \rightarrow {}^3F_{2,3}$ transition), in the spectral range well covered by high-power and high-brightness commercial ytterbium fiber lasers. This determines the suitability of this compound for ESA pumping. The first Tm:$CaGdAlO_4$ laser with dual-wavelength pumping at 1.05 µm is realized in the present work.

The first Tm:$CaGdAlO_4$ laser operating on the $^3H_4 \rightarrow {}^3H_5$ transition with a pure direct pumping at 0.79 µm generated 264 mW at 2301-2325 nm with a slope efficiency of 16.2% with respect to the incident pump power and 31.3% with respect to the absorbed pump power. The laser emission is linearly polarized (σ). Further improvement of the slope efficiency is expected via optimizing the Tm^{3+} doping level and power scaling for this pumping scheme is envisioned via diode-pumping by commercial spatially multimode AlGaAs laser diodes.

Finally, we have revealed the role of cascade laser on the $^3H_4 \rightarrow {}^3H_5$ and $^3F_4 \rightarrow {}^3H_6$ Tm^{3+} transitions on the 2.3 µm laser performance of Tm-lasers. Under pure direct pumping, by allowing the cascade laser at 1.77 µm and 2.32 µm, the bottleneck effect related to accumulation of electronic excitations in the intermediate long-living $^3F_4$ Tm^{3+} state was efficiently avoided (the $^3F_4 \rightarrow {}^3H_6$ laser transition drained the $^3F_4$ manifold) thus avoiding the excessive ground-state ($^3H_6$) bleaching and increasing the pump absorption. Under dual-wavelength pumping at 0.79 and 1.05 µm combining both the direct and UC pumping schemes, it was possible to tune the power ratio between the 1.77 and 2.32 µm laser emissions by varying the UC pump power. The latter was because of the recirculation of the $^3F_4$ population in favor of the $^3H_4$ one by the $^3F_4 \rightarrow {}^3F_{2,3}$ ESA process.

Optics EXPRESS

We believe that the different experiments described in this article would help in the future development of 2.3 µm Tm:CALGO lasers whose interest consists in having a broad emission favorable to tunable and ultrashort-pulse laser development in this spectral range.

Funding. Agence Nationale de la Recherche.

Disclosures. The authors declare no conflicts of interest.

Data availability. Data underlying the results presented in this paper are not publicly available at this time but may be obtained from the authors upon reasonable request.

References

1. F. J. McAleavey, J. O'Gorman, J. F. Donegan, B. D. MacCraith, J. Hegarty, and G. Maze, "Narrow linewidth, tunable Tm^{3+}-doped fluoride fiber laser for optical-based hydrocarbon gas sensing," IEEE J. Sel. Top. Quantum Electron. **3**(4), 1103–1111 (1997).
2. G. G. Taylor, D. Morozov, N. R. Gemmell, K. Erotokritou, S. Miki, H. Terai, and R. H. Hadfield, "Photon counting LIDAR at 2.3 µm wavelength with superconducting nanowires," Opt. Express **27**(26), 38147–38158 (2019).
3. V. Petrov, "Frequency down-conversion of solid-state laser sources to the mid-infrared spectral range using non-oxide nonlinear crystals," Progr. Quantum Electron. **42**, 1–106 (2015).
4. J. F. Pinto, L. Esterowitz, and G. H. Rosenblatt, "Tm^{3+}:YLF laser continuously tunable between 2.20 and 2.46 µm," Opt. Lett. **19**(12), 883–885 (1994).
5. P. Loiko, R. Soulard, L. Guillemot, G. Brasse, J.-L. Doulan, A. Braud, A. Tyazhev, A. Hideur, B. Guichardaz, F. Druon, and P. Camy, "Efficient Tm:$LiYF_4$ lasers at ~2.3 µm: Effect of energy-transfer upconversion," IEEE J. Quantum Electron. **55**(6), 1–12 (2019).
6. F. Zha, X. Yu, H. Chu, H. Pan, S. Zhao, P. Loiko, Z. Pan, and D. Li, "Compact diode-pumped continuous wave and passively Q switched Tm:YAG laser at 2.33 µm," Opt. Lett. **47**(23), 6265–6268 (2022).
7. I. Yorulmaz and A. Sennaroglu, "Low-threshold diode-pumped 2.3-µm Tm^{3+}:YLF lasers," IEEE J. Sel. Top. Quantum Electron. **24**(5), 1–7 (2018).
8. L. Guillemot, P. Loiko, R. Soulard, A. Braud, J.-L. Doualan, A. Hideur, and P. Camy, "Close look on cubic Tm:KY_3F_{10} crystal for highly efficient lasing on the $^3H_4 \rightarrow {}^3H_5$ transition," Opt. Express **28**(3), 3451–3463 (2020).
9. P. Loiko, E. Kifle, L. Guillemot, J.-L. Doualan, F. Starecki, A. Braud, M. Aguiló, F. Díaz, V. Petrov, X. Mateos, and P. Camy, "Highly efficient 2.3 µm thulium lasers based on a high-phonon-energy crystal: evidence of vibronic-assisted emissions," J. Opt. Soc. Am. B **38**(2), 482–495 (2021).
10. L. Guillemot, P. Loiko, A. Braud, J.-L. Doualan, A. Hideur, M. Koselja, R. Moncorge, and P. Camy, "Continuous-wave Tm:$YAlO_3$ laser at ~2.3 µm," Opt. Lett. **44**(20), 5077–5080 (2019).
11. L. Guillemot, P. Loiko, R. Soulard, A. Braud, J.-L. Doualan, A. Hideur, R. Moncorgé, and P. Camy, "Thulium laser at ~2.3 µm based on upconversion pumping," Opt. Lett. **44**(16), 4071–4074 (2019).
12. R. M. El-Agmy and N. M. Al-Hosiny, "2.31 µm laser under up-conversion pumping at 1.064 µm in Tm^{3+}: ZBLAN fibre lasers," Electron. Lett. **46**(13), 936–937 (2010).
13. M. F. Joubert, S. Guy, B. Jacquier, and C. Linares, "The photon-avalanche effect: review, model and application," Opt. Mater. **4**(1), 43–49 (1994).
14. Y. Morova, M. Tonelli, V. Petrov, and A. Sennaroglu, "Upconversion pumping of a 2.3 µm Tm^{3+}: KY_3F_{10} laser with a 1064 nm ytterbium fiber laser," Opt. Lett. **45**(4), 931–934 (2020).
15. Y. Morova, E. N. Kamun, M. Tonelli, and A. Sennaroglu, "Tunable laser operation of Tm^{3+}:KY_3F_{10} near 1.9 µm via upconversion pumping at 1064 nm," J. Opt. Soc. Am. B **38**(8), B21–B25 (2021).
16. A. Tyazhev, P. Loiko, L. Guillemot, A. Kouta, R. M. Solé, X. Mateos, M. Aguiló, F. Díaz, H. Dupont, P. Georges, F. Druon, A. Braud, P. Camy, and A. Hideur, "Excited-state absorption and upconversion pumping of Tm3+-doped potassium lutetium double tungstate," Opt. Express (*accepted*, 2023).
17. Y. H. Tsang, D. J. Coleman, and T. A. King, "High power 1.9 µm Tm^{3+}- silica fibre laser pumped at 1.09 µm by a Yb^{3+}-silica fibre laser," Opt. Commun. **231**(1-6), 357–364 (2004).
18. J. Wang, Z. Jia, Y. Mei, C. Zhang, F. Wang, Y. Sun, Y. Ohishi, W. Qin, and G. Qin, "2.3 µm lasing in Tm^{3+} doped fluoroaluminate glass fibers with an upconversion pumping scheme," Opt. Mater. Express **13**(3), 764–770 (2023).
19. A. Tyazhev, F. Starecki, S. Cozic, P. Loiko, L. Guillemot, A. Braud, F. Joulain, M. Tang, T. Godin, A. Hideur, and P. Camy, "Watt-level efficient 2.3 µm thulium fluoride fiber laser," Opt. Lett. **45**(20), 5788–5791 (2020).
20. H. Dupont, L. Guillemot, P. Loiko, A. Braud, J.-L. Doualan, P. Camy, P. Georges, and F. Druon, "Dual-wavelength-pumping of mid-infrared Tm:YLF laser at 2.3 µm: demonstration of pump seeding and recycling processes," Opt. Express **30**(18), 32141–32150 (2022).
21. F. Wang, H. Huang, H. Chen, Y. Bao, Z. Li, and D. Shen, "GSA and ESA dual-wavelength pumped 2.3 µm Tm:YLF laser on the $^3H_4 \rightarrow {}^3H_5$ transition," Chin. Opt. Lett. **19**(9), 091405 (2021).
22. B. Schmaul, G. Huber, R. Clausen, B. Chai, P. LiKamWa, and M. Bass, "Er^{3+}:$YLiF_4$ continuous wave cascade laser operation at 1620 and 2810 nm at room temperature," Appl. Phys. Lett. **62**(6), 541–543 (1993).
23. L. Esterowitz, R. C. Eckardt, and R. E. Allen, "Long-wavelength stimulated emission via cascade laser action in Ho:YLF," Appl. Phys. Lett. **35**(3), 236–239 (1979).

Optics EXPRESS

24. S. Tessarin, M. Lynch, J. F. Donegan, and G. Maze, "Tm^{3+}-doped ZBLAN fibre amplifier at 1.49 µm with co-operative lasing at 1.88 µm," Electron. Lett. **41**(16), 899–900 (2005).
25. G. Kintz, R. Allen, and L. Esterowitz, "cw and pulsed 2.8 µm laser emission from diode-pumped Er^{3+}:$LiYF_4$ at room temperature," Appl. Phys. Lett. **50**(22), 1553–1555 (1987).
26. P. S. Golding, S. D. Jackson, T. A. King, and M. Pollnau, "Energy transfer processes in Er^{3+}-doped and Er^{3+}, Pr^{3+}-codoped ZBLAN glasses," Phys. Rev. B **62**(2), 856–864 (2000).
27. M. Pollnau, T. Graf, J. E. Balmer, W. Lüthy, and H. P. Weber, "Explanation of the cw operation of the Er^{3+} 3-µm crystal laser," Phys. Rev. A **49**(5), 3990–3996 (1994).
28. S. Ye, X. Zhou, S. Huang, H. Nie, J. Bian, T. Li, K. Yang, J. He, and B. Zhang, "Cascade MIR Ho:YLF laser at 2.1 µm and 2.9 µm," Opt. Lett. **47**(21), 5642–5645 (2022).
29. S. Sujecki, L. Sójka, E. Bereś-Pawlik, Z. Tang, D. Furniss, A. B. Seddon, and T. M. Benson, "Modelling of a simple Dy^{3+} doped chalcogenide glass fibre laser for mid-infrared light generation," Opt. Quantum Eletcron. **42**(2), 69–79 (2010).
30. R. Soulard, A. Tyazhev, J. L. Doualan, A. Braud, A. Hideur, M. Laroche, B. Xu, and P. Camy, "2.3 µm Tm^{3+}:YLF mode-locked laser," Opt. Lett. **42**(18), 3534–3536 (2017).
31. F. Canbaz, I. Yorulmaz, and A. Sennaroglu, "Kerr-lens mode-locked 2.3-µm Tm^{3+}:YLF laser as a source of femtosecond pulses in the mid-infrared," Opt. Lett. **42**(19), 3964–3967 (2017).
32. P. O. Petit, J. Petit, P. Goldner, and B. Viana, "Inhomogeneous broadening of optical transitions in Yb:$CaYAlO_4$," Opt. Mater. **30**(7), 1093–1097 (2008).
33. P. Loiko, F. Druon, P. Georges, B. Viana, and K. Yumashev, "Thermo-optic characterization of Yb:$CaGdAlO_4$ laser crystal," Opt. Mater. Express **4**(11), 2241–2249 (2014).
34. F. Druon, M. Olivier, A. Jaffrès, P. Loiseau, N. Aubry, J. DidierJean, F. Balembois, B. Viana, and P. Georges, "Magic mode switching in Yb:$CaGdAlO_4$ laser under high pump power," Opt. Lett. **38**(20), 4138–4141 (2013).
35. Y. Zaouter, J. Didierjean, F. Balembois, G. Lucas Leclin, F. Druon, P. Georges, J. Petit, P. Goldner, and B. Viana, "47-fs diode-pumped Yb^{3+}:$CaGdAlO_4$ laser," Opt. Lett. **31**(1), 119–121 (2006).
36. P. Sévillano, P. Georges, F. Druon, D. Descamps, and E. Cormier, "32-fs Kerr-lens mode-locked Yb:$CaGdAlO_4$ oscillator optically pumped by a bright fiber laser," Opt. Lett. **39**(20), 6001–6004 (2014).
37. Y. Wang, X. Su, Y. Xie, F. Gao, S. Kumar, Q. Wang, C. Liu, B. Zhang, B. Zhang, and J. He, "17.8 fs broadband Kerr-lens mode-locked Yb:CALGO oscillator," Opt. Lett. **46**(8), 1892–1895 (2021).
38. E. Talik, J. Kisielewski, P. Zajdel, A. Guzik, E. Wierzbicka, A. Kania, J. Kusz, S. Miga, and M. Szubka, "XPS spectroscopy, structural, magnetic and dielectric investigations of $CaGdAlO_4$ and Yb:$CaGdAlO_4$ single crystals," Opt. Mater. **91**, 355–362 (2019).
39. Z. Pan, P. Loiko, J. M. Serres, E. Kifle, H. Yuan, X. Dai, H. Cai, Y. Wang, Y. Zhao, M. Aguiló, F. Díaz, U. Griebner, V. Petrov, and X. Mateos, ""Mixed" Tm:Ca(Gd,Lu)AlO_4 - a novel crystal for tunable and mode-locked 2 µm lasers," Opt. Express **27**(7), 9987 (2019).
40. Y. Wang, G. Xie, X. Xu, J. Di, Z. Qin, S. Suomalainen, M. Guina, A. Härkönen, A. Agnesi, U. Griebner, X. Mateos, P. Loiko, and V. Petrov, "SESAM mode-locked Tm:CALGO laser at 2 µm," Opt. Mater. Express **6**(1), 131–136 (2016).
41. Y. Wang, P. Loiko, Y. Zhao, Z. Pan, W. Chen, M. Mero, X. Xu, J. Xu, X. Mateos, A. Major, M. Guina, V. Petrov, and U. Griebner, "Polarized spectroscopy and SESAM mode-locking of Tm,Ho:CALGO," Opt. Express **30**(5), 7883–7893 (2022).
42. P. Loiko, P. Becker, L. Bohatý, C. Liebald, M. Peltz, S. Vernay, D. Rytz, J. M. Serres, X. Mateos, Y. Wang, X. Xu, J. Xu, A. Major, A. Baranov, U. Griebner, and V. Petrov, "Sellmeier equations, group velocity dispersion and thermo-optic dispersion formulas for $CaLnAlO_4$ (Ln = Y, Gd) laser host crystals," Opt. Lett. **42**(12), 2275–2278 (2017).
43. L. Guillemot, P. Loiko, J.-L. Doualan, A. Braud, and P. Camy, "Excited-state absorption in thulium-doped materials in the near-infrared," Opt. Express **30**(18), 31669–31684 (2022).
44. B. Aull and H. Jenssen, "Vibronic interactions in Nd:YAG resulting in nonreciprocity of absorption and stimulated emission cross sections," IEEE J. Quantum Electron. **18**(5), 925–930 (1982).
45. P. Loiko and M. Pollnau, "Stochastic model of energy-transfer processes among rare-earth ions. Example of Al_2O_3:Tm^{3+}," J. Phys. Chem. C **120**(46), 26480–26489 (2016).
46. V. Llamas, P. Loiko, and E. Kifle, *et al.*, "Ultrafast laser inscribed waveguide lasers in Tm:CALGO with depressed-index cladding," Opt. Express **28**(3), 3528–3540 (2020).
47. F. Wang, H. Huang, F. Wu, H. Chen, Y. Bao, Z. Li, O. L. Antipov, S. S. Balabanov, and D. Shen, "2.3–2.5 µm laser operation of LD-pumped Tm:YAP on the $^3H_4 \rightarrow {}^3H_5$ transition," Opt. Mater. **115**, 111054 (2021).